



## Research article

# Aqueous-phase room-temperature afterglow crystalline micro/nanostructures via supramolecular inclusion complexation of $\gamma$ -cyclodextrin with difluoroboron $\beta$ -diketonate luminescence compounds

Qianqian Yan, Junbo Li, Tengyue Wang, Wen Xia, Guangming Wang, Haodong Li, Kaka Zhang <sup>\*</sup>

*State Key Laboratory of Organometallic Chemistry and Shanghai Hongkong Joint Laboratory in Chemical Synthesis, Key Laboratory of Synthetic and Self-Assembly Chemistry for Organic Functional Molecules, Ningbo Zhongke Creation Center of New Materials, Shanghai Institute of Organic Chemistry, University of Chinese Academy of Sciences, Chinese Academy of Sciences, 345 Lingling Road, Shanghai 200032, PR China*



## ARTICLE INFO

**Keywords:**

Aqueous  
Organic afterglow  
Room temperature phosphorescence  
 $\gamma$ -cyclodextrin  
Difluoroboron  $\beta$ -diketonate  
Inclusion complexation

## ABSTRACT

Room-temperature phosphorescence and organic afterglow materials exhibit significant applications in diverse fields. Among them, aqueous-phase organic afterglow materials display interesting biomedical and other applications, whereas afterglow material fabrication in aqueous medium remains less explored when compared to those in solid states. In view of the excellent afterglow performance in difluoroboron  $\beta$ -diketonate containing systems, here we report supramolecular inclusion complexation of  $\gamma$ -cyclodextrin ( $\gamma$ CD) with difluoroboron  $\beta$ -diketonate ( $\text{BF}_2\text{bdk}$ ) phosphors for devising aqueous-phase room-temperature afterglow crystalline micro/nanostructures. The  $\gamma$ CD- $\text{BF}_2\text{bdk}$  host-guest supramolecular interactions induce crystallization of the two-component system into micro/nanostructures where  $\text{BF}_2\text{bdk}$ 's triplet excited states can be well protected from nonradiative decay and oxygen quenching, leading to the emergence of aqueous-phase afterglow with phosphorescence lifetimes around 1 s and high photoluminescence quantum yields ( $\text{PLQY} > 50\%$ ). The aqueous afterglow materials possess visible-light-excitable property and can serve as donor of energy transfer for constructing long-wavelength and color-tunable afterglow systems. Their potential applications for bioimaging were further demonstrated. The present study provides a simple method but a new avenue for the preparation of high-performance aqueous-phase afterglow materials.

## 1. Introduction

The room temperature phosphorescence (RTP) and organic afterglow materials have great applications in anti-counterfeiting, biological imaging, organic light-emitting diodes and so on because of their long triplet lifetime nature [1–16]. In recent years, numerous RTP materials have been fabricated and widely developed [1–22]. Of particular interest, the room-temperature afterglow materials in aqueous phase have drawing increasing attention for their potential biological applications [23–26]. For instance, recent studies show that core-shell polymer nanoparticles crosslinked with phosphors were designed for the detection of dissolved oxygen [27]. The formation of nanoparticles through the self-assembled dimers produced aqueous phase RTP materials for bioimaging under visible and near-infrared irradiation [28]. Besides, a red-emissive RTP molecule has been synthesized by introducing an alkoxy spacer group to modulate the intermolecular electronic coupling

and the heavy atom effects (HAE) independently. The formation of RTP materials in aqueous media through nanocrystalline strategy was investigated, showing excellent biocompatibility [29]. The aqueous afterglow dispersions prepared by top-down method for *in vivo* bio-imaging were also reported. Following irradiation with a UV lamp, these dispersions were injected into nude mice in bioluminescent mode [30]. However, it remains challenging to realize long-lived aqueous phase afterglow in air because of the non-radiative decay and oxygen quenching.

Methods such as mechanical grinding [31,32], sonication treatment [30,33], nanoprecipitation [34–36], supramolecular host-guest inclusion complexation [37,38], emulsion polymerization [39–41] and melt droplet emulsification [42,43] have been used to fabricate aqueous afterglow dispersions. Techniques such as mechanical grinding and sonication treatment have been employed to facilitate the aqueous dispersion of crystalline afterglow compounds with the aid of

\* Corresponding author.

E-mail address: [zhangkaka@sioc.ac.cn](mailto:zhangkaka@sioc.ac.cn) (K. Zhang).

surfactants to enhance water dispersibility and stability. In the nano-precipitation approach, solid-state afterglow materials dissolved in organic solvents were introduced into water, leading to the formation of micro/nanoparticles characterized by well-defined morphologies and controlled size distributions. Based on a dopant-matrix design strategy and emulsion polymerization technique, where dopants were dissolved in monomers and polymer latex particles were formed by emulsion polymerization, aqueous afterglow dispersions under degassed condition were fabricated due to the non-radiative decay was dramatically suppressed. Additionally, supramolecular host-guest inclusion complexation has emerged as an effective strategy to construct RTP materials in aqueous media, owing to the hydrophilic nature of the exterior of host molecules [5,44,45]. Macro cyclic molecules, such as cucurbituril and cyclodextrin, can form stable host-guest inclusion complexes with the phosphors. The cavities of hosts provide rigid microenvironments for phosphors to suppress the non-radiative transition caused by molecular vibration. For instance, the photocontrolled reversible RTP materials have been demonstrated in aqueous solutions through the complexation of  $\beta$ CD and guests [46]. Moreover, visible-light-excitable afterglow materials based on the host-guest system with quaternary stacking structures were fabricated utilizing cucurbit[8]uril (CB[8]) as the host and a positively charged triazine derivative as the guest [47]. A water-soluble supramolecular polymer exhibiting a phosphorescence lifetimes ( $\tau_p$ ) of 4.33 ms was achieved by the combination of CBs and luminophore-conjugated hyaluronic acid (HA) [48]. A light-harvesting phosphorescence energy transfer system in aqueous solution was constructed based on the CB[8] and heavy-atom modified  $\beta$ CD [49]. In addition, RTP materials of host-guest inclusion of  $\gamma$ CD with negatively charged molecules in aqueous solution was reported, where careful molecular design is crucial to avoid oxygen quenching [50]. To date, despite these advancements, most  $\tau_p$  of reported aqueous phase RTP materials are still limited to microseconds to milliseconds, with seconds ultralong lifetimes are rarely reported due to the non-radiative decay and oxygen quenching in aqueous media. Recently, an aqueous phase RTP material based on the host-guest inclusion and intermolecular hydrogen bonding interactions of  $\beta$ CD and  $\beta$ -biphenylboronic acid was reported, achieving an impressive lifetime of 1.03 s under 280 nm UV light excitation [33].

Previous studies by others and our group show that BF<sub>2</sub>bdk compounds display excellent RTP properties [28,35,51–57]. It was reported that the aqueous dispersion of polylactic acid (PLA) systems with end-capped BF<sub>2</sub>bdk moieties was fabricated as fluorescence/phosphorescence ratiometric sensors for hypoxia mapping and promising cancer diagnosis [52]. Additionally, the nanocrystals from donor-acceptor (D-A) molecules of BF<sub>2</sub>bdk derivatives prepared by micelle-assisted assembly method were employed to fabricate a long-lived aqueous phase RTP under visible light excitation [35]. A twisted D-A-D molecule composing of BF<sub>2</sub>bdk and carbazole units was designed with an afterglow efficiency up to 45 % and nanoparticles dispersed in water were prepared for bioimaging and multicolour visual sensing of temperature [51]. It has been found in our systematic studies that the T<sub>n</sub> states ( $n = 2$  or 3) can mediate BF<sub>2</sub>bdk's S<sub>1</sub>-to-T<sub>1</sub> intersystem crossing because of the El-Sayed rule and the energy gap rule [56,57]. The afterglow emulsions of BF<sub>2</sub>bdk compounds prepared by emulsion polymerization or melt droplet emulsification exhibit diverse advantages, including long lifetime, stimuli-responsiveness, long-wavelength emission, and good biorecognition properties, showing promising biological applications [39, 40,58]. Notably, to our knowledge, the inclusion complexation of BF<sub>2</sub>bdk and supramolecular host has not been reported in literature.

Since water and oxygen are ubiquitous in biological systems, the development of visible-light-excitable, long-lived aqueous-phase afterglow materials under aerobic conditions is significant for their potential applications in biology. According to the formula of  $\tau_p = 1/(k_p + k_{nr} + k_q)$ , where  $k_p$ ,  $k_{nr}$  and  $k_q$  are the rate constants of phosphorescence decay, non-radiative decay and oxygen quenching, respectively, the diminished  $k_p$  and suppressed  $k_{nr} + k_q$  are essential to fabricate long-

lived RTP materials. We reason that it is crucial to sufficiently suppress  $k_{nr}$  and protect triplets from quenchers. Pioneer studies show that supramolecular hosts play a pivotal role to effectively protect triplet excitons and inhibit  $k_{nr}$  and  $k_q$  via host-guest interactions, hydrogen bonding and so on [59–64]. While, if the micro/nanocrystals of inclusion complexes can be generated in aqueous media to further stabilize triplet excitons, is it possible to realize ultralong lifetime aqueous phase afterglow materials in air?

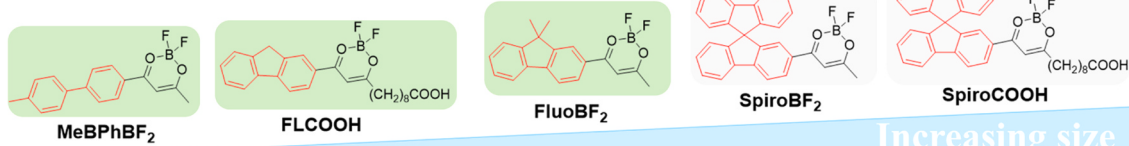
In view of above design strategy, here we report the successful fabrication of long-lived aqueous-phase afterglow materials based on the supramolecular self-assembly of  $\gamma$ CD and BF<sub>2</sub>bdk compounds exhibiting intramolecular charge transfer (ICT) characters. The micro/nanocrystalline inclusion complexes in aqueous solution were formed by straightforward admixture of stock solution of  $\gamma$ CD with suitable BF<sub>2</sub>bdk compound solution. The synergy of crystallinity and host-guest interactions efficiently decreased the value of  $k_{nr} + k_q$ . Consequently, it is found that the resultant afterglow materials exhibit ultralong green afterglow in air under visible light excitation with an ultralong  $\tau_p$  of around 1 s, alongside a high PLQY exceeding 50 %. Furthermore, when adding rhodamine 6 G (Rh6G) or rhodamine B (RhB) to the system, tunable long-wavelength emission afterglow materials were obtained via an energy transfer process. The preliminary bioimaging studies of the afterglow suspensions show their potential applications in biology.

## 2. Results and discussion

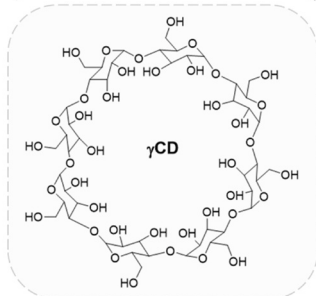
The macrocyclic molecules CD (i.e.  $\alpha$ CD,  $\beta$ CD,  $\gamma$ CD), which are composed of glucose units, have a hydrophobic cavity and hydrophilic outer surface, as well as abundant hydroxyl. They can form stable host-guest inclusion complexes with neutral or negatively charged guests in aqueous solution through supramolecular interactions such as electrostatic interaction, hydrogen bonding and hydrophobic effect [45,65,66]. In this study, natural  $\gamma$ CD with relatively large hydrophobic cavity and good water solubility is used as the host. A series of biphenyl/fluorene-containing BF<sub>2</sub>bdk derivatives with different sizes were selected as guests, which are named as MeBPF<sub>2</sub>, FLCOOH, FluoBF<sub>2</sub>, SpiroBF<sub>2</sub>, and SpiroCOOH, respectively (Scheme 1A). The synthesis of the five BF<sub>2</sub>bdk compounds was followed by the same procedures reported by our group [54–56]. The structures of the compounds were characterized by <sup>1</sup>H NMR, <sup>13</sup>C NMR, <sup>11</sup>B NMR, <sup>19</sup>F NMR, ESI-MS, FT-IR and their high purity was further confirmed by HPLC (Supporting Information, Figure S46–S74). BF<sub>2</sub>bdk compounds in dichloromethane solution show strong UV-vis absorption bands from 300 nm to 420 nm (Figure S2, Table S1) and intense emission band from 400 nm to 550 nm (Figure S3, Table S1). The BF<sub>2</sub>bdk compounds in solution or solid states show absence of afterglow under ambient conditions.

For the fabrication of afterglow materials in aqueous solution, the BF<sub>2</sub>bdk compounds of FLCOOH and FluoBF<sub>2</sub> were first tested to self-assemble with  $\gamma$ CD. High-concentration solutions of  $\gamma$ CD in water and BF<sub>2</sub>bdk in acetonitrile were prepared. As depicted in Scheme 1C, one drop of BF<sub>2</sub>bdk solution was added into the  $\gamma$ CD solution, where the mass ratio of BF<sub>2</sub>bdk: $\gamma$ CD = 1:99. The solution became turbid immediately. Surprisingly, the obtained aqueous suspension of FLCOOH- $\gamma$ CD-1 % exhibits blue emission under the UV light irradiation, and after ceasing the UV light, it exhibits intense green afterglow with a duration of 5 s under ambient conditions (Fig. 1A). The FluoBF<sub>2</sub>- $\gamma$ CD-1 % suspension also exhibits intense blue emission and green afterglow up to 9 s (Fig. 1B). Such long-lived and air-insensitive aqueous-phase afterglow materials are rarely reported. Moreover, after centrifuging, the precipitate exhibits intense afterglow (Figure S4). However, it is insoluble in water and acetonitrile. After adding water, a kind of uniformly dispersed afterglow material in water is obtained. Based on the above results, we propose that the assemblies were formed contributed to the host-guest interactions. The hydrophilic surface of  $\gamma$ CD allows the system to disperse in water. The cavity of  $\gamma$ CD provided a rigid microenvironment

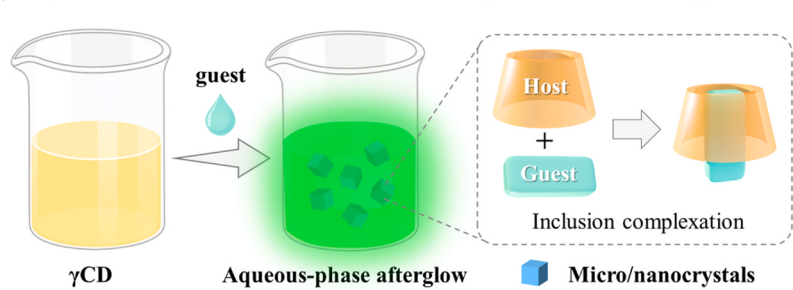
## (A) Luminophores/Guest



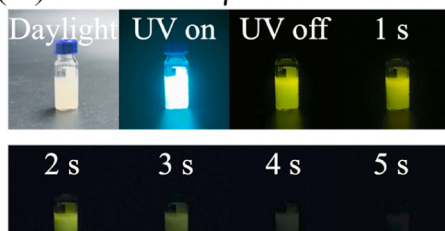
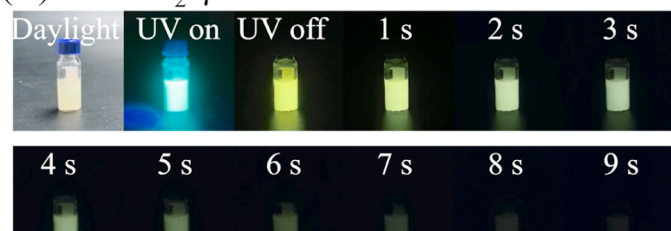
## (B) Host



## (C) Crystalline micro/nanostructures via host-guest inclusion complexation



**Scheme 1.** Chemical structures of (A) the luminophores in the present study and (B)  $\gamma$ CD. (C) Schematic of the formation of aqueous RTP materials with crystalline micro/nanostructures based on the supramolecular inclusion complexation of luminophores and  $\gamma$ CD.

(A) FLCOOH- $\gamma$ CD-1%(B) FluoBF<sub>2</sub>- $\gamma$ CD-1%(C) FLCOOH- $\gamma$ CD(D) FluoBF<sub>2</sub>- $\gamma$ CD

**Fig. 1.** The photographs of (A) FLCOOH- $\gamma$ CD-1 % aqueous suspension, (B) FluoBF<sub>2</sub>- $\gamma$ CD-1 % aqueous suspension, (C) FLCOOH- $\gamma$ CD suspensions at different concentrations and (D) FluoBF<sub>2</sub>- $\gamma$ CD suspensions at different concentrations under the daylight, 365 nm UV light irradiation and after ceasing the light source.

for the guests and dramatically suppressed the non-radiative decay of the guests and avoided the oxygen quenching.

Following the same procedures, the BF<sub>2</sub>bdk- $\gamma$ CD-0.1 % and BF<sub>2</sub>bdk- $\gamma$ CD-0.01 % suspensions were prepared, where the mass ratio of BF<sub>2</sub>bdk and  $\gamma$ CD is 1:1000 and 1:10000, respectively. BF<sub>2</sub>bdk- $\gamma$ CD-0.1 % with lower solid content show similar intense emission and afterglow with the BF<sub>2</sub>bdk- $\gamma$ CD-1 %. Besides, the suspensions BF<sub>2</sub>bdk- $\gamma$ CD-0.01 % with very low feed concentration of assemblies (0.01 wt%) still can exhibit afterglow (Fig. 1C and 1D).

Next, we investigated the photophysical properties of the afterglow materials. The UV-vis spectra of the suspensions show absorption bands from 300 nm to 500 nm, indicating that the suspensions are visible light excitable (Figure S11). The room-temperature steady-state emission spectra of FLCOOH- $\gamma$ CD show an emission band from 400 nm to 600 nm and show a slightly red shift when the concentration of FLCOOH is increased (Fig. 2A and S13A). Their delayed emission spectra (1 ms delay) show a band with the same shape and maxima of 545 nm (Fig. 2B and S13B), which originates from the room-temperature phosphorescence of FLCOOH. While, the emission intensity of FLCOOH- $\gamma$ CD-1 % is lower than FLCOOH- $\gamma$ CD-0.1 % suspension, which is probably due to

the strong light scattering in the suspension systems. The PLQY of FLCOOH- $\gamma$ CD-1 % was measured as high as 76.1 % (Table 1). After peak separation, the room-temperature steady-state emission spectra possess different ratios of fluorescence and phosphorescence components (Figure S14). The phosphorescence quantum yield ( $\Phi_p$ ) of the FLCOOH- $\gamma$ CD-1 % suspension can be estimated to be 28.4 %. The emission decay curves of FLCOOH- $\gamma$ CD-1 % follow exponential decay with a  $\tau_p$  of 0.54 s (Fig. 2C). When the concentration of FluoBF<sub>2</sub> is increased, the room-temperature steady-state emission spectra of FluoBF<sub>2</sub>- $\gamma$ CD also show a red shift of the peak from 495 nm to 513 nm (Fig. 3D and S13C) and the delayed emission spectra (1 ms delay) show an emission band at 544 nm (Fig. 3E and S13D). The emission decay curves show that FluoBF<sub>2</sub>- $\gamma$ CD-1 % sample has a  $\tau_p$  up to 0.95 s (Fig. 3F), which is among the longest phosphorescence lifetimes of reported aqueous-phase afterglow materials. The PLQY was measured to be 54.9 % and the  $\Phi_p$  can be estimated to be 23.0 % (Figure S14). The photophysical data were summarized in Table 1.

Moreover, we found that the afterglow suspensions exhibit afterglow after turning off the daylight (Fig. 3A-B), implying that the suspensions can be excited by visible light. The excitation spectra of FLCOOH- $\gamma$ CD-

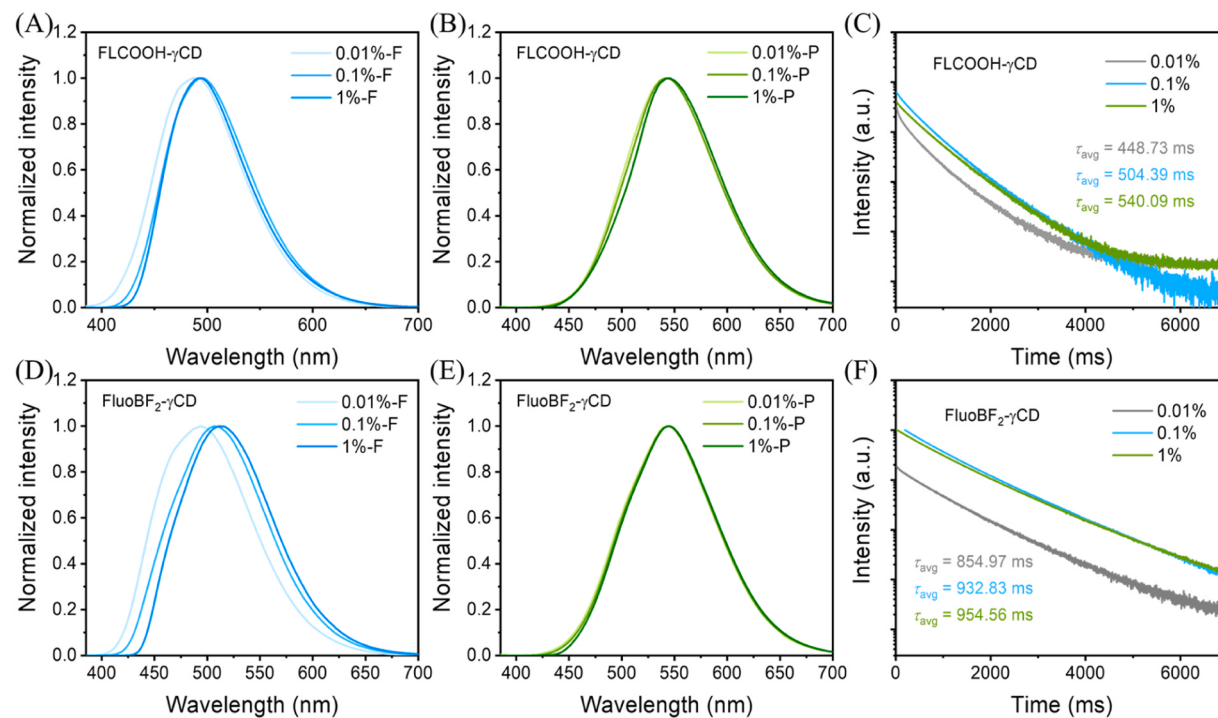


**Fig. 2.** (A) Room-temperature steady-state and (B) delayed emission (1 ms delay) spectra of FLCOOH- $\gamma$ CD suspensions with different mass ratios of FLCOOH- $\gamma$ CD. (C) Room-temperature decay profile of FLCOOH- $\gamma$ CD suspensions with different mass ratios of FLCOOH- $\gamma$ CD. (D) Room-temperature steady-state and (E) delayed emission (1 ms delay) spectra of FluoBF<sub>2</sub>- $\gamma$ CD suspensions with different mass ratios of FLCOOH- $\gamma$ CD. (F) Room-temperature decay profile of FluoBF<sub>2</sub>- $\gamma$ CD suspensions with different mass ratios of FLCOOH- $\gamma$ CD.

**Table 1**  
The photophysical properties of the afterglow materials.

Entry	$\lambda_F$ (nm)	$\lambda_P$ (nm)	$\Delta E_{ST}$ (eV)	$\tau_p$ (ms)	PLQY (%)
FLCOOH- $\gamma$ CD-0.01 %	488	545	0.27	448.73	-
FLCOOH- $\gamma$ CD-0.1 %	494	545	0.23	504.39	40.4
FLCOOH- $\gamma$ CD-1 %	494	545	0.23	540.09	76.1
FluoBF <sub>2</sub> - $\gamma$ CD-0.01 %	495	544	0.23	854.97	-
FluoBF <sub>2</sub> - $\gamma$ CD-0.1 %	508	544	0.16	932.83	38.2
FluoBF <sub>2</sub> - $\gamma$ CD-1 %	513	544	0.14	954.56	54.1

1 % and FluoBF<sub>2</sub>- $\gamma$ CD-1 % suspensions show wide bands from 280 nm to 450 nm (Figure S12). The room-temperature steady-state and delayed emission spectra (1 ms delay) excited at 420 nm show a similar emission band with the spectra excited at 365 nm (Fig. 3C, 3E and S31). Since the  $\gamma$ CD has negligible absorption over 300 nm, the triplet excited energy transfer from  $\gamma$ CD to BF<sub>2</sub>bdk compounds can be ruled out. The  $\tau_p$  of FLCOOH- $\gamma$ CD-1 % and FluoBF<sub>2</sub>- $\gamma$ CD-1 % samples monitored at 545 nm is 0.54 s (Fig. 3D) and 0.97 s (Fig. 3F), respectively.

In view of the fact that ultrasound treatment is beneficial to the uniform dispersion of nanoparticles, the experiments to prepare BF<sub>2</sub>bdk- $\gamma$ CD-1 % suspensions with ultrasound treatment were conducted. The obtained FLCOOH- $\gamma$ CD-1 % suspension showed similar optical properties with the suspension without ultrasound treatment (Figure S15). However, the emission intensity of FluoBF<sub>2</sub>- $\gamma$ CD-1 % suspension is decreased and phosphorescence lifetime are slightly shorter after ultrasound treatment (Figure S16).

We also investigated the stability of the afterglow suspensions. After stand for 1 h, the suspensions of FLCOOH- $\gamma$ CD-1 % and FluoBF<sub>2</sub>- $\gamma$ CD-1 % show different degrees of deposition (Figure S17-18). The FluoBF<sub>2</sub>- $\gamma$ CD-1 % was completely deposited after 2 h. FLCOOH- $\gamma$ CD-1 % was slowly deposited until it was completely deposited after 1 d, which might owe to the smaller particle size (*vide infra*). However, after shaking them again, the obtained uniform dispersed suspensions exhibiting the same deposition rate, indicating the formed micro-

nanoparticles remain almost same. Furthermore, preliminary bio-imaging studies of FluoBF<sub>2</sub>- $\gamma$ CD-1 % afterglow suspension were performed. When the FluoBF<sub>2</sub>- $\gamma$ CD-1 % suspension was injected into the living fish, the green afterglow can be observed with very clean background after UV light or visible light irradiation (Fig. 4), showing the potential applications of afterglow suspensions in high-contrast bioimaging.

Time-dependent density functional theory (TD-DFT) calculations show that the BF<sub>2</sub>bdk compounds possess typical ICT characters plus localized excitation (LE) characters (Figure S5-10). Unlike the HAE and n- $\pi^*$  transition that can increase  $k_{ISC}$  and  $k_p$  simultaneously, the organic luminescent compounds with ICT characteristic can reduce  $\Delta E_{ST}$ , leading to the increase of  $k_{ISC}$  values to realize high-efficient RTP materials and showing less effect on  $k_p$ . Besides, since the  $k_p$  follows the order of  ${}^3LE < {}^3ICT < {}^3n-\pi^*$ , the existence of  ${}^3LE$  characters in organic T<sub>1</sub> states can result in small  $k_p$ , leading to long  $\tau_p$ . Take FLCOOH as an example, the  $\Delta E_{ST}$  in S<sub>1</sub>-T<sub>2</sub> and S<sub>1</sub>-T<sub>3</sub> ISC channels is smaller than the S<sub>1</sub>-T<sub>1</sub> ISC channel (Figure S6). The spin-orbit coupling matrix elements (SOCME) value of FLCOOH in S<sub>1</sub>-T<sub>2</sub> ISC channel reaches to 1.05 cm<sup>-1</sup>, larger than in S<sub>1</sub>-T<sub>1</sub> ISC channel. According to El-Sayed rule and the energy gap law, the S<sub>1</sub>-T<sub>1</sub> and S<sub>1</sub>-T<sub>3</sub> ISC channels can mediate BF<sub>2</sub>bdk's ISC process and remarkably populate organic triplets. The  $\Delta E_{ST}$  value estimated from fluorescence and phosphorescence maxima is only 0.23 eV (Table 1). Similarly, the FluoBF<sub>2</sub> molecule also shows strong ISC tendency, which is necessary for high phosphorescence quantum yield (Figure S7). In addition, the host-guest system of FluoBF<sub>2</sub> and  $\gamma$ CD was further studied by ONIOM calculation to consider the effect of  $\gamma$ CD environments on the photophysical properties of BF<sub>2</sub>bdk molecule (Figure S10). The calculated S<sub>1</sub> state energy level of the host guest compound is lower than the FluoBF<sub>2</sub> molecule while the T<sub>1</sub> state energy level is less changed, leading to a smaller  $\Delta E_{ST}$  value in the host-guest system. Besides, there are also rich ISC channels with reasonable SOCME values. These can explain the excellent population of T<sub>1</sub> states in the FluoBF<sub>2</sub>- $\gamma$ CD system.

The morphologies of the samples in suspension were characterized

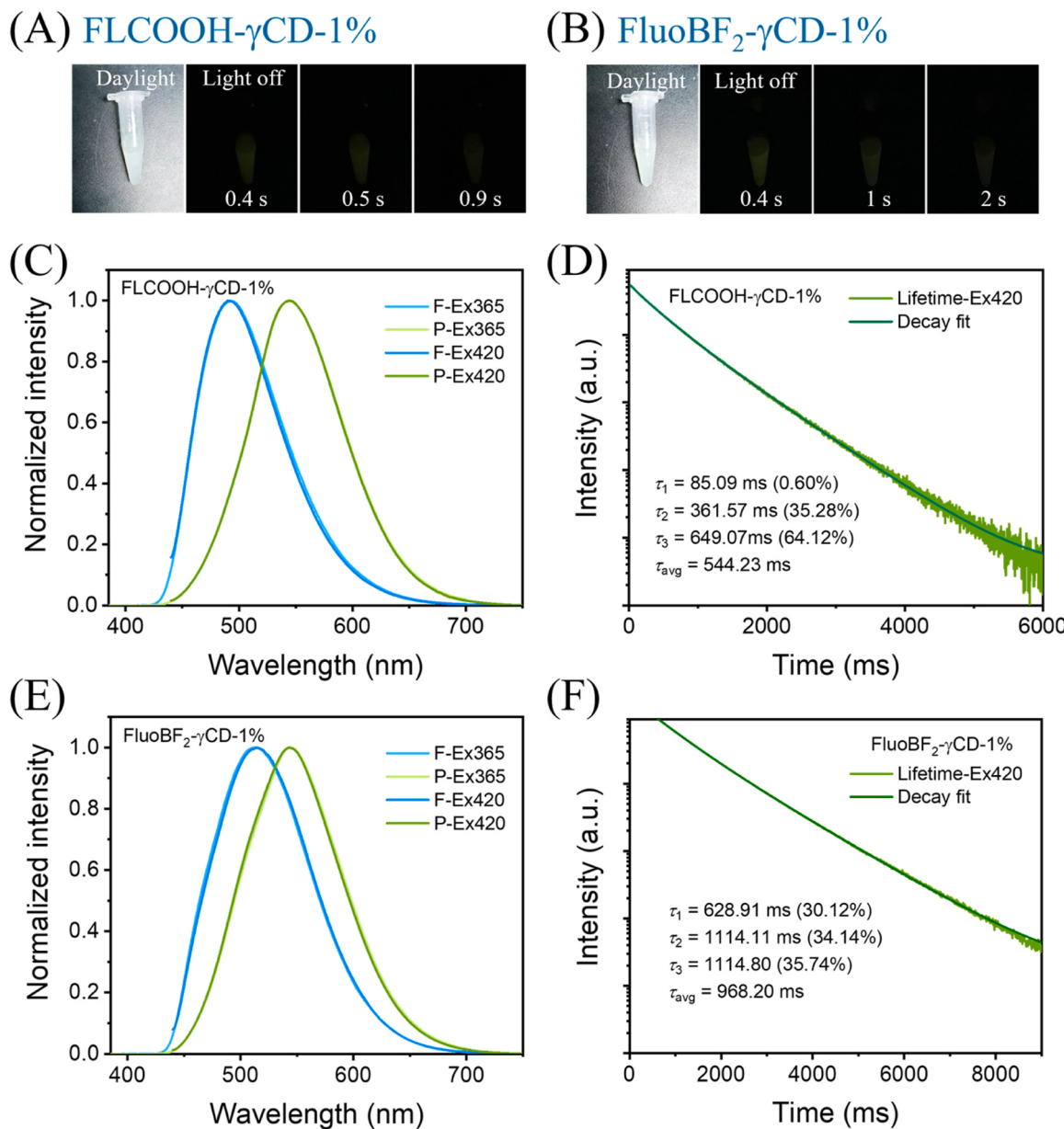


**Fig. 3.** Photographs of aqueous solutions of (A) FLCOOH- $\gamma$ CD-1 % suspensions and (B) FluoBF<sub>2</sub>- $\gamma$ CD-1 % under the daylight after turning off the light. (C) Room-temperature steady-state (blue line) and delayed emission (1 ms delay, green line) spectra of FLCOOH- $\gamma$ CD-1 % suspensions excited at 365 nm and 420 nm, respectively. (D) Room-temperature decay profile of FLCOOH- $\gamma$ CD-1 % suspensions excited at 420 nm. (E) Room-temperature steady-state (blue line) and delayed emission (1 ms delay, green line) spectra of FluoBF<sub>2</sub>- $\gamma$ CD-1 % suspensions excited at 365 nm and 420 nm, respectively. (F) Room-temperature decay profile of FluoBF<sub>2</sub>- $\gamma$ CD-1 % suspensions excited at 420 nm.

by scanning electron microscope (SEM). Notably, different with the micron-sized blocks of  $\gamma$ CD and FLCOOH, the FLCOOH- $\gamma$ CD-1 % shows regular square micro-nanoparticles with an average size approximately 255 nm (Fig. 5A-C). The formation of crystalline particles was evidenced by powder X-ray diffraction (PXRD) results (Fig. 5D). Similar results were found from the FluoBF<sub>2</sub>- $\gamma$ CD-1 % materials (Figure S19-20), proving the formation of micro/nanocrystalline particles in their aqueous solutions. The crystalline structures can further suppress the  $k_{\text{nr}}$ , contributing to the long  $\tau_p$  in aqueous solution.

Furthermore, the MeBPBF<sub>2</sub>- $\gamma$ CD-1 % afterglow suspension is also fabricated by using relatively small molecule MeBPBF<sub>2</sub> as the guest (Figure S21), which can be also excited by visible light (Figure S22-23, Table S2). The PLQY is up to 75.4 % and  $\Phi_p$  is around 27.5 % (Figure S14). However, when the solution of SpiroBF<sub>2</sub> or SpiroCOOH was added into the  $\gamma$ CD solution, although the solution became a bit

turbid, no afterglow can be observed (Figure S24-25). We speculate that the assemblies of  $\gamma$ CD with SpiroBF<sub>2</sub> or SpiroCOOH were not formed due to the guests are too large to be encapsulated, or  $\gamma$ CD has a very weak restriction effect on the molecular vibration of SpiroBF<sub>2</sub> or SpiroCOOH.

To validate our hypothesis, more experiments were performed. The powders or crystals of BF<sub>2</sub>bdk compounds exhibit no afterglow after UV light excitation. For the construction of afterglow materials, we also tried to utilize the well-developed dopant-matrix design strategy. The powder of  $\gamma$ CD and solution of the FluoBF<sub>2</sub> in dichloromethane were added into an agate mortar, and then FluoBF<sub>2</sub> compound was doped into  $\gamma$ CD by grinding at 1 % doping concentration. The obtained powders exhibit intense blue emission (Figure S26-27). However, no afterglow was observed after excited by 365 nm UV light (Figure S26B). In the same way, the mixed powders of  $\gamma$ CD and other BF<sub>2</sub>bdk compounds also exhibit negligible afterglow (Figure S26), suggesting that  $\gamma$ CD can't

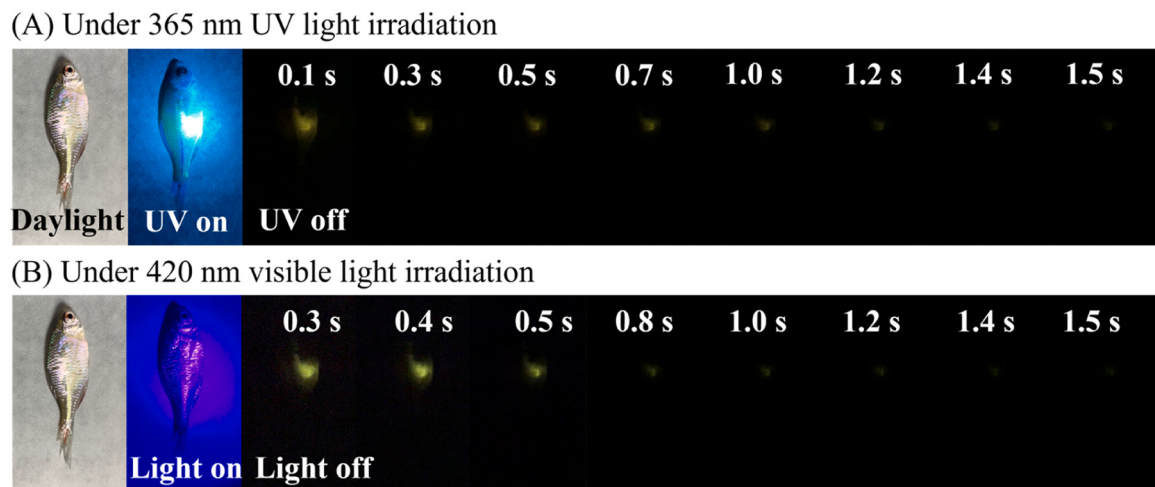


**Fig. 4.** Preliminary bioimaging studies of FluoBF<sub>2</sub>- $\gamma$ CD-1 % afterglow suspension. Photographs of living fish injected FluoBF<sub>2</sub>- $\gamma$ CD-1 % suspension under daylight, (A) 365 nm UV light or (B) 420 nm visible light and after turning off the lamp.

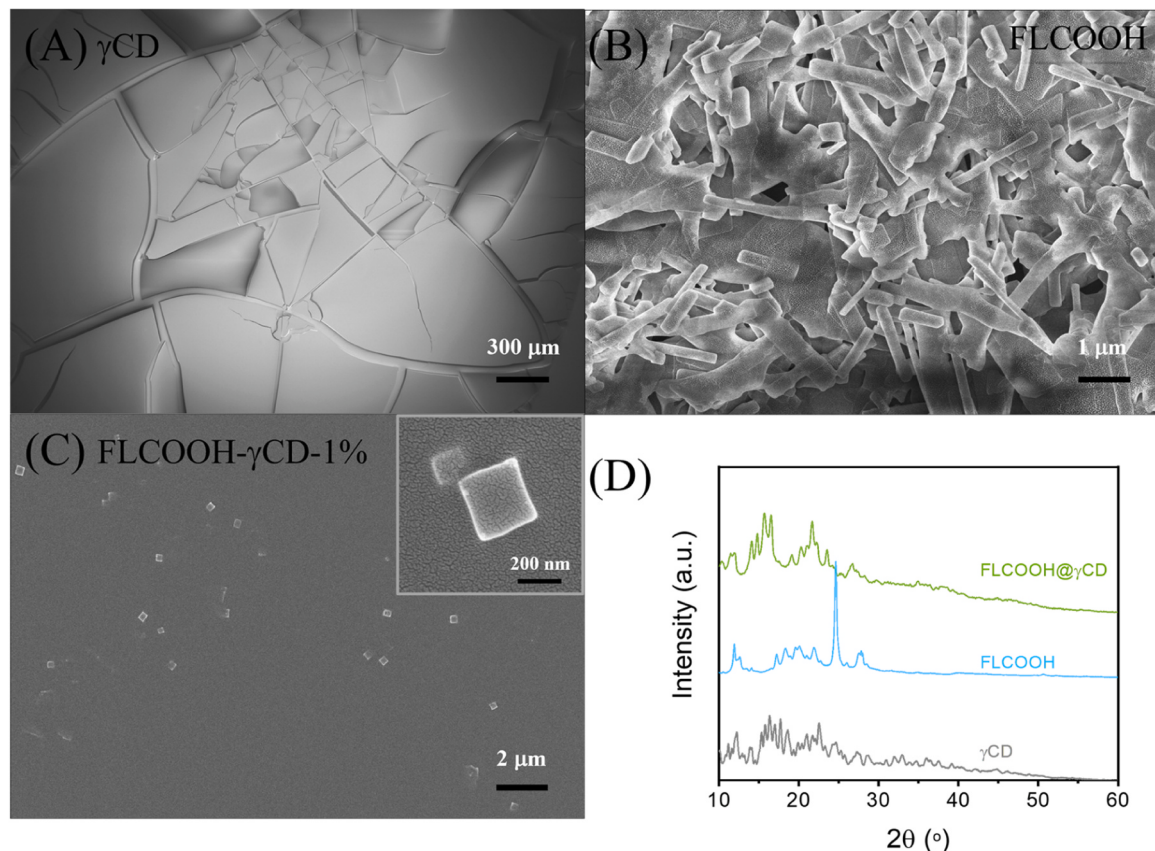


**Fig. 5.** SEM images of (A)  $\gamma$ CD (B) FLCOOH and (C) FLCOOH- $\gamma$ CD-1 % in the dried states. (D) PXRD patterns of  $\gamma$ CD, FLCOOH, and FLCOOH- $\gamma$ CD-1 % afterglow materials in the dried states.

protect the triplets well by simply physical mixing of the luminophores and  $\gamma$ CD. As a control, the BF<sub>2</sub>bdk-H<sub>2</sub>O suspensions without  $\gamma$ CD were also prepared by adding BF<sub>2</sub>bdk solution to water following the same procedure as BF<sub>2</sub>bdk- $\gamma$ CD-1 %. The suspensions show intense emission under 365 nm UV light, but no afterglow can be observed after ceasing light source (Figure S28). These observations are consisting with their spectral results (Figure S29-31).

Unfortunately, the efforts to grow crystals are unsuccessful, as well as the NMR titrations experiments, due to the poor solubility of the

assemblies in water. To further confirm the formation of the assembly, the precipitates of FLCOOH- $\gamma$ CD-1 %, FluoBF<sub>2</sub>- $\gamma$ CD-1 % and SpiroBF<sub>2</sub>- $\gamma$ CD-1 % were collected and dissolved in deuterated dimethyl sulfoxide (DMSO-*d*<sub>6</sub>). From the <sup>1</sup>H NMR spectra of FluoBF<sub>2</sub>- $\gamma$ CD-1 %-precipitate, both signals of  $\gamma$ CD and FluoBF<sub>2</sub> were found and the ratio of  $\gamma$ CD and the guests is approximately 1.3:1, respectively (Figure S75), confirming the self-assembly of the guests and  $\gamma$ CD. Fourier transform infrared (FT-IR) spectra were also recorded (Figure S32-34). FluoBF<sub>2</sub>- $\gamma$ CD-1 %-precipitate displays almost identical bands with  $\gamma$ CD. The characteristic band at

$3374\text{ cm}^{-1}$  corresponds to vibration of OH group. Comparing with the mixed powder of FluoBF<sub>2</sub> and  $\gamma$ CD with the molar ratio of 1:2, the signals from FluoBF<sub>2</sub> of FluoBF<sub>2</sub>- $\gamma$ CD-1 %-precipitate are still much weaker, probably due to the encapsulation of  $\gamma$ CD. A weak band at  $1540\text{ cm}^{-1}$  can be assigned to the vibration of dioxaborine ring from FluoBF<sub>2</sub>. Similar results were observed from the spectra of FLCOOH- $\gamma$ CD-1 %-precipitate, further proving the assembly of  $\gamma$ CD and the guests. Besides, the  $\gamma$ CD solution remains clear when only mixed with the same amount of acetonitrile solvent (Figure S36). Therefore, it can be ruled out that the  $\gamma$ CD is precipitate by the addition of acetonitrile. It is worth to note that the <sup>1</sup>H NMR spectrum of SpiroBF<sub>2</sub>- $\gamma$ CD-1 %-precipitate only showed the signal of SpiroBF<sub>2</sub> without  $\gamma$ CD (Figure S76). Thus, the formation of suspension is due to the poor solubility of the SpiroBF<sub>2</sub> in  $\gamma$ CD aqueous solution rather than self-assembly with  $\gamma$ CD.

Meanwhile, the BF<sub>2</sub>bdk-free compound 2-acetylfluorene (Afluo) was also used as a guest to prepare the afterglow solution of the Afluo- $\gamma$ CD-1 %. The obtained suspension exhibit afterglow with a duration less than 1 s (Figure S37). The <sup>1</sup>H NMR spectrum of Afluo- $\gamma$ CD-1 %-precipitate show that the integral ratio of Afluo and  $\gamma$ CD is 1:0.92 (Figure S77), indicating that the fluorene moiety is crucial to binding with the  $\gamma$ CD through host-guest interactions such as hydrophobic interactions, hydrogen bonding, etc.

Interestingly, the delayed emission spectra of FLCOOH- $\gamma$ CD-1 % and FluoBF<sub>2</sub>- $\gamma$ CD-1 % suspensions have a good overlap with the absorption spectra of Rhodamine B (RhB) and Rhodamine 6 G (Rh6G) in aqueous solution (Fig. 6). It would be suitable to produce long-wavelength afterglow materials via an energy transfer process. Inspired by this, Rh6G and RhB were chosen as energy acceptors to construct the long-wavelength afterglow systems.

When the aqueous solution of Rh6G and RhB were added into the FluoBF<sub>2</sub>- $\gamma$ CD-1 % suspension at 1 wt% concentration (the mass ratio of dyes and the FluoBF<sub>2</sub> is 1:1), respectively, the orange-colored

suspension of FluoBF<sub>2</sub>- $\gamma$ CD-1 %-Rh6G and red-colored suspension of FluoBF<sub>2</sub>- $\gamma$ CD-1 %-RhB were obtained (Fig. 7A-B). They exhibit intense orange or red emission under 365 nm UV light irradiation and after turning off the light with an afterglow duration of around 7 s (Fig. 7A-B). The steady-state spectra excited at 420 nm of FluoBF<sub>2</sub>- $\gamma$ CD-1 %-Rh6G and FluoBF<sub>2</sub>- $\gamma$ CD-1 %-RhB show similar bands with their delayed spectra, which can be assigned to Rh6G and RhB (Fig. 7C-D). The delayed spectra (1 ms delay) of FluoBF<sub>2</sub>- $\gamma$ CD-1 %-Rh6G or FluoBF<sub>2</sub>- $\gamma$ CD-1 %-RhB display a main peak at 590 nm and 624 nm, respectively (Fig. 7C-D), indicating the highly effective energy transfer from the donor to acceptor (Rh6G or RhB). The energy transfer efficiencies were estimated to be approximately 99 % according to the equation of  $\Phi_{ET} = 1 - A/A_0$ , where  $A$  and  $A_0$  refer to the integral area of the emission band of the donor with and without acceptors (Figure S45) [67]. When 0.01 wt % and 0.1 % of RhB were added into the FluoBF<sub>2</sub>- $\gamma$ CD-1 % suspensions, there are two peaks with different intensity in their delayed spectra, indicating the tunable emission colors can also achieved by mixing the different ratio of the guests and dyes (Figure S38-40). The FLCOOH- $\gamma$ CD-1 %-Rh6G and FLCOOH- $\gamma$ CD-1 %-RhB also manifest highly efficient energy transfer, exhibiting orange and red afterglow, respectively (Figure S41-44, Table S3).

### 3. Conclusion

In summary, we have developed a simple method for the effective fabrication of long-lived aqueous-phase afterglow materials through the supramolecular inclusion complexation of  $\gamma$ CD and neutral BF<sub>2</sub>bdk compounds. The host-guest interactions, coupled with the formation of micro/nanocrystalline particles, significantly suppressed the non-radiative decay of the guests and avoid the oxygen quenching. The obtained aqueous phase afterglow materials can be excited by visible light, exhibiting ultralong green afterglow with a phosphorescence lifetime

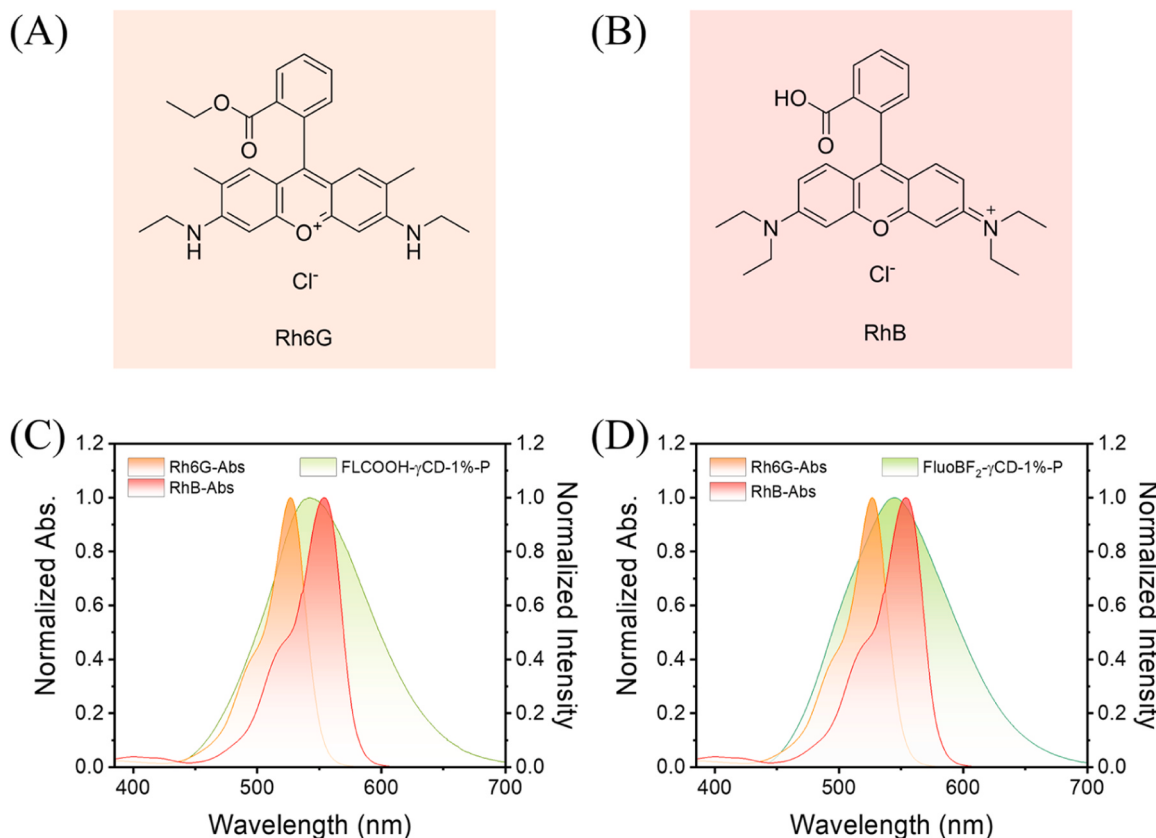


**Fig. 6.** Chemical structures of (A) rhodamine 6 G and (B) rhodamine B. (C) Absorption spectra of Rh6G and RhB and room-temperature delayed emission spectrum (1 ms delay) of FLCOOH- $\gamma$ CD-1 %. (D) Absorption spectra of Rh6G and RhB and room-temperature delayed emission (1 ms delay) of FluoBF<sub>2</sub>- $\gamma$ CD-1 %.

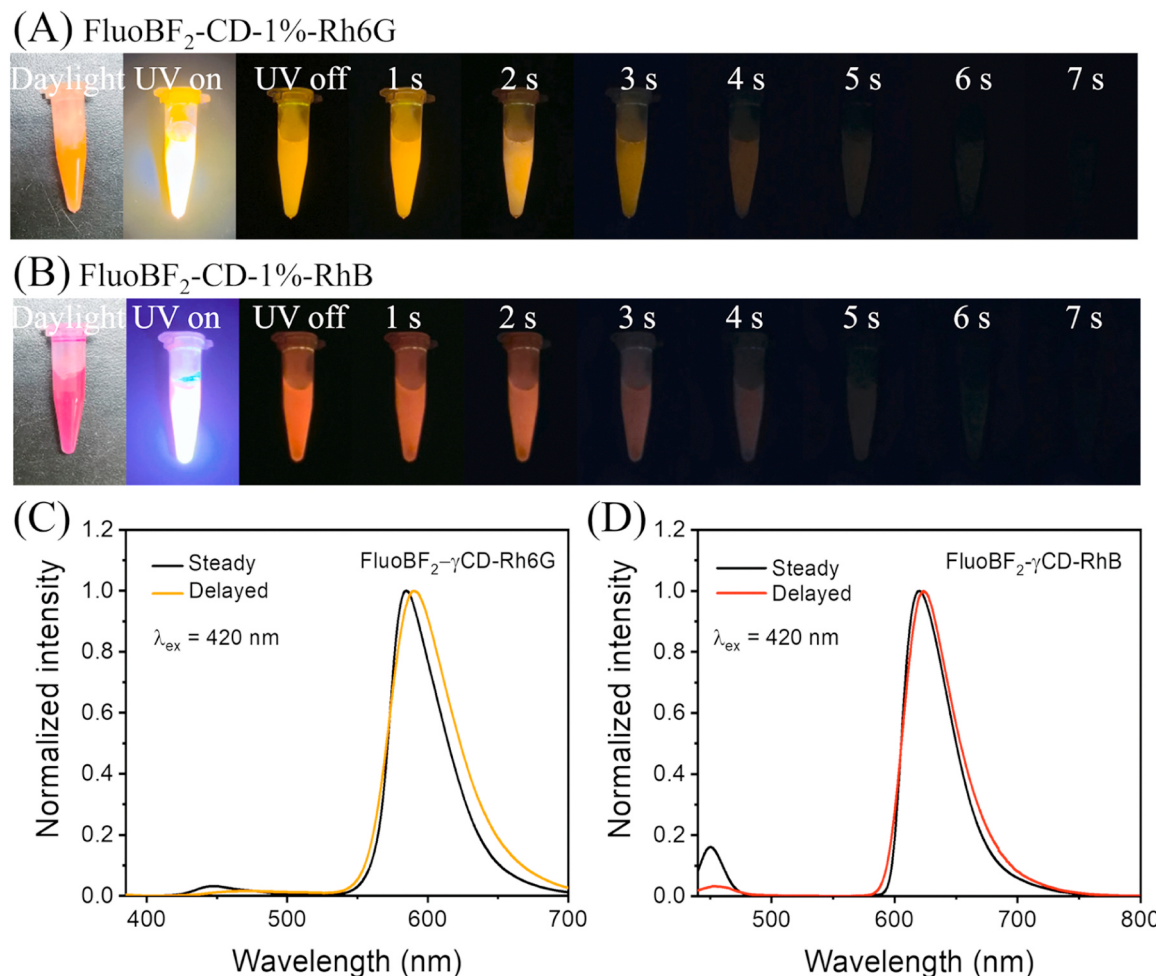


**Fig. 7.** Photographs of aqueous suspensions of (A) FluoBF<sub>2</sub>-γCD-1 %-Rh6G and (B) FluoBF<sub>2</sub>-γCD-1 %-RhB under the daylight, 365 nm UV light irradiation and after ceasing the light source. (C) Room-temperature steady-state (black line) and delayed emission (1 ms delay, orange line) spectra of FluoBF<sub>2</sub>-γCD-1 %-Rh6G suspension excited at 420 nm. (D) Room-temperature steady-state (black line) and delayed emission (1 ms delay, red line) spectra of FluoBF<sub>2</sub>-γCD-1 %-RhB suspension excited at 420 nm.

approximately 1 s in air and showing potential applications in bio-imaging. Furthermore, the addition of Rh6G or RhB enables tunable emission colors and long-wavelength emission afterglow through highly efficient energy transfer. This work provides a new strategy to develop the RTP materials and prepare high-performance aqueous-phase RTP materials.

#### Declaration of Competing Interest

The authors declare that they have no known competing financial interests or personal relationships that could have appeared to influence the work reported in this paper.

#### Acknowledgements

We thank the financial supports from National Natural Science Foundation of China (22175194), the Strategic Priority Research Program of the Chinese Academy of Sciences (XDB0610000), Hundred Talents Program from Shanghai Institute of Organic Chemistry (Y121078), Pioneer Hundred Talents Program of Chinese Academy of Sciences (E320021), and Ningbo Natural Science Foundation (2023J243).

#### Appendix A. Supporting information

Supplementary data associated with this article can be found in the online version at [doi:10.1016/j.nxmate.2024.100379](https://doi.org/10.1016/j.nxmate.2024.100379).

#### References

- [1] V.W.-W. Yam, V.K.-M. Au, S.Y.-L. Leung, Light-emitting self-assembled materials based on d<sup>8</sup> and d<sup>10</sup> transition metal complexes, *Chem. Rev.* 115 (2015) 7589–7728, <https://doi.org/10.1021/acs.chemrev.5b00074>.
- [2] R. Kabe, C. Adachi, Organic long persistent luminescence, *Nature* 550 (2017) 384–387, <https://doi.org/10.1038/nature24010>.
- [3] W. Zhao, Z. He, B.Z. Tang, Room-temperature phosphorescence from organic aggregates, *Nat. Rev. Mater.* 5 (2020) 869–885, <https://doi.org/10.1038/s41578-020-0223-z>.
- [4] N. Gan, H. Shi, Z. An, W. Huang, Recent advances in polymer-based metal-free room-temperature phosphorescent materials, *Adv. Funct. Mater.* 28 (2018) 1802657, <https://doi.org/10.1002/adfm.201802657>.
- [5] X. Ma, J. Wang, H. Tian, Assembling-induced emission: an efficient approach for amorphous metal-free organic emitting materials with room-temperature phosphorescence, *Acc. Chem. Res.* 52 (2019) 738–748, <https://doi.org/10.1021/acs.accounts.8b00620>.
- [6] Kenry, C. Chen, B. Liu, Enhancing the performance of pure organic room-temperature phosphorescent luminophores, *Nat. Commun.* 10 (2019) 2111, <https://doi.org/10.1038/s41467-019-10033-2>.
- [7] S. Hirata, Recent advances in materials with room-temperature phosphorescence: photophysics for triplet exciton stabilization, *Adv. Opt. Mater.* 5 (2017) 1700116, <https://doi.org/10.1002/adom.201700116>.
- [8] Y. Zhang, Y. Su, H. Wu, Z. Wang, C. Wang, Y. Zheng, et al., Large-area, flexible, transparent, and long-lived polymer-based phosphorescence films, *J. Am. Chem. Soc.* 143 (2021) 13675–13685, <https://doi.org/10.1021/jacs.1c05213>.

- [9] Z. Xu, Y. He, H. Shi, Z. An, Room-temperature phosphorescence materials from crystalline to amorphous state, *SmartMat* 4 (2023) e1139, <https://doi.org/10.1002/smm.21139>.
- [10] Y. Zhang, H. Li, M. Yang, W. Dai, J. Shi, B. Tong, et al., Organic room-temperature phosphorescence materials for bioimaging, *Chem. Commun.* 59 (2023) 5329–5342, <https://doi.org/10.1039/D3CC00923H>.
- [11] J. Wang, Y. Yang, K. Li, L. Zhang, Z. Li, Purely organic fluorescence afterglow: visible-light-excitation, inherent mechanism, tunable color, and practical applications with very low cost, *Angew. Chem. Int. Ed.* 62 (2023) e202304020, <https://doi.org/10.1002/anie.202304020>.
- [12] Y. Zhou, W. Qin, C. Du, H. Gao, F. Zhu, G. Liang, Long-lived room-temperature phosphorescence for visual and quantitative detection of oxygen, *Angew. Chem. Int. Ed.* 58 (2019) 12102–12106, <https://doi.org/10.1002/anie.201906312>.
- [13] F. Lin, H. Wang, Y. Cao, R. Yu, G. Liang, H. Huang, et al., Stepwise energy transfer: near-infrared persistent luminescence from doped polymeric systems, *Adv. Mater.* 34 (2022) 2108333, <https://doi.org/10.1002/adma.202108333>.
- [14] X. Yang, G.I.N. Waterhouse, S. Lu, J. Yu, Recent advances in the design of afterglow materials: mechanisms, structural regulation strategies and applications, *Chem. Soc. Rev.* 52 (2023) 8005–8058, <https://doi.org/10.1039/D2CS00993E>.
- [15] C. Xing, Z. Qi, B. Zhou, D. Yan, W. Fang, Solid-state photochemical cascade process boosting smart ultralong room-temperature phosphorescence in bismuth halides, *Angew. Chem. Int. Ed.* 63 (2024) e202402634, <https://doi.org/10.1002/anie.202402634>.
- [16] L. Shi, J. Liu, L. Ma, Y. Wang, The dual-band emission with long-lived thermally activated delayed fluorescence and room temperature phosphorescence by trace ingredient incorporation, *Chem. Eng. J.* 493 (2024) 152492, <https://doi.org/10.1016/j.cej.2024.152492>.
- [17] J. Guo, J. Liu, Y. Zhao, Y. Wang, L. Ma, J. Jiang, Time-dependent and clustering-induced phosphorescence, mechanochromism, structural-function relationships, and advanced information encryption based on isomeric effects and host–guest doping, *Spectrochim. Acta A Mol. Biomol. Spectrosc.* 317 (2024) 124449, <https://doi.org/10.1016/j.saa.2024.124449>.
- [18] F. Nie, D. Yan, Zero-dimensional halide hybrid bulk glass exhibiting reversible photochromic ultralong phosphorescence, *Nat. Commun.* 15 (2024) 5519, <https://doi.org/10.1038/s41467-024-49886-7>.
- [19] B. Zhou, Glassy inorganic-organic hybrid materials for photonic applications, *Matter* 7 (2024) 1–27, <https://doi.org/10.1016/j.matt.2024.04.004>.
- [20] C. Xing, B. Zhou, D. Yan, W. Fang, Integrating full-color 2D optical waveguide and heterojunction engineering in halide microsheets for multichannel photonic logical gates, *Adv. Sci.* 11 (2024) 2310262, <https://doi.org/10.1002/advs.202310262>.
- [21] C. Xing, B. Zhou, D. Yan, W.-H. Fang, Dynamic photoresponsive ultralong phosphorescence from one-dimensional halide microrods toward multilevel information storage, *CCS Chem.* 5 (2023) 2866–2876, <https://doi.org/10.31635/ccschem.023.202202605>.
- [22] X. Fang, Y. Tang, Y.-J. Ma, G. Xiao, P. Li, D. Yan, Ultralong-lived triplet excitons of room-temperature phosphorescent carbon dots located on g-C<sub>3</sub>N<sub>4</sub> to boost photocatalysis, *Sci. China Mater.* 66 (2022) 664–671, <https://doi.org/10.1007/s40843-022-2163-9>.
- [23] H. Sun, L. Zhu, Achieving purely organic room temperature phosphorescence in aqueous solution, *Aggregate* 4 (2023) e253, <https://doi.org/10.1002/agt2.253>.
- [24] W. Luo, J. Zhou, Y. Nie, F. Li, S. Cai, G. Yin, et al., Hydrogen-bonded organic frameworks enabling highly robust aqueous phase ultralong room-temperature phosphorescence, *Adv. Funct. Mater.* (2024) 2401728, <https://doi.org/10.1002/adfm.202401728>.
- [25] M. Ji, X. Ma, Recent progress with the application of organic room-temperature phosphorescent materials, *Ind. Chem. Mater.* 1 (2023) 582–594, <https://doi.org/10.1039/D3IM00004D>.
- [26] S. Garain, B.C. Garain, M. Eswaramoorthy, S.K. Pati, S.J. George, Light-harvesting supramolecular phosphors: highly efficient room temperature phosphorescence in solution and hydrogels, *Angew. Chem. Int. Ed.* 60 (2021) 19720–19724, <https://doi.org/10.1002/anie.202107295>.
- [27] Y. Yu, M.S. Kwon, J. Jung, Y. Zeng, M. Kim, K. Chung, et al., Room-temperature-phosphorescence-based dissolved oxygen detection by core-shell polymer nanoparticles containing metal-free organic phosphors, *Angew. Chem. Int. Ed.* 56 (2017) 16207–16211, <https://doi.org/10.1002/anie.201708606>.
- [28] X.-F. Wang, H. Xiao, P.-Z. Chen, Q.-Z. Yang, B. Chen, C.-H. Tung, et al., Pure organic room temperature phosphorescence from excited dimers in self-assembled nanoparticles under visible and near-infrared irradiation in water, *J. Am. Chem. Soc.* 141 (2019) 5045–5050, <https://doi.org/10.1021/jacs.9b00859>.
- [29] S.M.A. Fateminia, Z. Mao, S. Xu, Z. Yang, Z. Chi, B. Liu, Organic nanocrystals with bright red persistent room-temperature phosphorescence for biological applications, *Angew. Chem. Int. Ed.* 56 (2017) 12160–12164, <https://doi.org/10.1002/anie.201705945>.
- [30] X. Chen, Y. Tao, Z. An, P. Chen, C. Xu, R. Chen, et al., Ultralong phosphorescence of water-soluble organic nanoparticles for in vivo afterglow imaging, *Adv. Mater.* 29 (2017) 1606665, <https://doi.org/10.1002/adma.201606665>.
- [31] B. Zhou, G. Wang, X. Wang, W. Guo, J. Li, K. Zhang, Highly efficient room-temperature organic afterglow achieved by collaboration of luminescent dimeric TADF dopants and rigid matrices, *J. Mater. Chem. C* 9 (2021) 3939–3947, <https://doi.org/10.1039/dtco5464j>.
- [32] X. Wang, J. Li, Y. Zeng, X. Chen, M. Wu, G. Wang, et al., Merging thermally activated delayed fluorescence and two-photon ionization mechanisms for highly efficient and ultralong-lived organic afterglow, *Chem. Eng. J.* 460 (2023) 141916, <https://doi.org/10.1016/j.cej.2023.141916>.
- [33] D. Li, Z. Liu, M. Fang, J. Yang, B.Z. Tang, Z. Li, Ultralong room-temperature phosphorescence with second-level lifetime in water based on cyclodextrin supramolecular assembly, *ACS Nano* 17 (2023) 12895–12902, <https://doi.org/10.1021/acsnano.3c04971>.
- [34] Z. An, C. Zheng, Y. Tao, R. Chen, H. Shi, T. Chen, et al., Stabilizing triplet excited states for ultralong organic phosphorescence, *Nat. Mater.* 14 (2015) 685–690, <https://doi.org/10.1038/nmat4259>.
- [35] X. Wang, W. Guo, H. Xiao, Q. Yang, B. Chen, Y. Chen, et al., Pure organic room temperature phosphorescence from unique micelle-assisted assembly of nanocrystals in water, *Adv. Funct. Mater.* 30 (2020) 1907282, <https://doi.org/10.1002/adfm.201907282>.
- [36] X. Liu, K. Zhang, J. Gao, Y. Chen, C. Tung, L. Wu, Monochromophore-based phosphorescence and fluorescence from pure organic assemblies for ratiometric hypoxia detection, *Angew. Chem. Int. Ed.* 59 (2020) 23456–23460, <https://doi.org/10.1002/anie.202007039>.
- [37] X. Yan, H. Peng, Y. Xiang, J. Wang, L. Yu, Y. Tao, et al., Recent advances on host–guest material systems toward organic room temperature phosphorescence, *Small* 18 (2022) 2104073, <https://doi.org/10.1002/smll.202104073>.
- [38] G. Yin, J. Zhou, W. Lu, L. Li, D. Liu, M. Qi, et al., Targeting compact and ordered emitters by supramolecular dynamic interactions for high-performance organic ambient phosphorescence, *Adv. Mater.* (2024) 2311347, <https://doi.org/10.1002/adma.202311347>.
- [39] J. Liu, Y. Sun, G. Wang, X. Chen, J. Li, X. Wang, et al., Organic afterglow emulsions exhibiting 2.4 s phosphorescence lifetimes and specific protein binding property, *Adv. Opt. Mater.* 10 (2022) 2201502, <https://doi.org/10.1002/adom.202201502>.
- [40] X. Zhai, Y. Zeng, X. Deng, Q. Lou, A. Cao, L. Ji, et al., Visible-light-excitable aqueous afterglow exhibiting long emission wavelength and ultralong afterglow lifetime of 7.64 s, *Chem. Commun.* 59 (2023) 10500–10503, <https://doi.org/10.1039/D3CC03288D>.
- [41] J. Huang, X. Deng, J. Li, G. Wang, X. Li, H. Yao, et al., Developing robust organic afterglow emulsion for dissolved oxygen sensing, *Chem. Eng. J.* 474 (2023) 145809, <https://doi.org/10.1016/j.cej.2023.145809>.
- [42] G. Wang, X. Chen, J. Liu, S. Ding, K. Zhang, Advanced charge transfer technology for highly efficient and long-lived TADF-type organic afterglow with near-infrared light-excitable property, *Sci. China Chem.* 66 (2023) 1120–1131, <https://doi.org/10.1007/s11426-022-1432-y>.
- [43] X. Deng, J. Huang, J. Li, G. Wang, K. Zhang, Sonication-responsive organic afterglow emulsions, *Adv. Funct. Mater.* 33 (2023) 2214960, <https://doi.org/10.1002/adfm.202214960>.
- [44] X.-Y. Dai, M. Huo, Y. Liu, Phosphorescence resonance energy transfer from purely organic supramolecular assembly, *Nat. Rev. Chem.* 7 (2023) 854–874, <https://doi.org/10.1038/s41570-023-00555-1>.
- [45] X.-K. Ma, Y. Liu, Supramolecular purely organic room-temperature phosphorescence, *Acc. Chem. Res.* 54 (2021) 3403–3414, <https://doi.org/10.1021/acs.accounts.1c00336>.
- [46] X. Ma, J. Cao, Q. Wang, H. Tian, Photocontrolled reversible room temperature phosphorescence (RTP) encoding β-cyclodextrin pseudorotaxane, *Chem. Commun.* 47 (2011) 3559, <https://doi.org/10.1039/c0cc05488g>.
- [47] J. Wang, Z. Huang, X. Ma, H. Tian, Visible-light-excited room-temperature phosphorescence in water by cucurbit[8]uril-mediated supramolecular assembly, *Angew. Chem. Int. Ed.* 59 (2020) 9928–9933, <https://doi.org/10.1002/anie.201914513>.
- [48] X. Zhou, X. Bai, F. Shang, H.-Y. Zhang, L.-H. Wang, X. Xu, et al., Supramolecular assembly activated single-molecule phosphorescence resonance energy transfer for near-infrared targeted cell imaging, *Nat. Commun.* 15 (2024) 4787, <https://doi.org/10.1038/s41467-024-49238-5>.
- [49] F.-F. Shen, Y. Chen, X. Dai, H.-Y. Zhang, B. Zhang, Y. Liu, et al., Purely organic light-harvesting phosphorescence energy transfer by β-cyclodextrin pseudorotaxane for mitochondria targeted imaging, *Chem. Sci.* 12 (2021) 1851–1857, <https://doi.org/10.1039/D0SC05343K>.
- [50] M. Hayduk, T. Schaller, F.C. Niemeyer, K. Rudolph, G.H. Clever, F. Rizzo, et al., Phosphorescence induction by host-guest complexation with cyclodextrins – the role of regioisomerism and affinity, *Chem. Eur. J.* 28 (2022) e202201081, <https://doi.org/10.1002/chem.202201081>.
- [51] H. Ma, L. Fu, X. Yao, X. Jiang, K. Lv, Q. Ma, et al., Boosting organic phosphorescence in adaptive host-guest materials by hyperconjugation, *Nat. Commun.* 15 (2024) 3660, <https://doi.org/10.1038/s41467-024-47992-0>.
- [52] G. Zhang, G.M. Palmer, M.W. Dewhurst, C.L. Fraser, A dual-emissive-materials design concept enables tumour hypoxia imaging, *Nat. Mater.* 8 (2009) 747–751, <https://doi.org/10.1038/nmat2509>.
- [53] X. Wang, Y. Sun, G. Wang, J. Li, X. Li, K. Zhang, TADF-type organic afterglow, *Angew. Chem. Int. Ed.* 60 (2021) 17138–17147, <https://doi.org/10.1002/anie.202105628>.
- [54] Y. Sun, J. Liu, J. Li, X. Li, X. Wang, G. Wang, et al., Manipulation of triplet excited states for long-lived and efficient organic afterglow, *Adv. Opt. Mater.* 10 (2022) 2101909, <https://doi.org/10.1002/adom.202101909>.
- [55] T. Wang, X. Wang, Q. Yan, K. Zhang, Ultralong organic room-temperature phosphorescence modulated by balancing intramolecular charge transfer and localized excitation character of excited states, *Dyes Pigments* 224 (2024) 112024, <https://doi.org/10.1016/j.dyepig.2024.112024>.
- [56] J. Li, W. Xia, J. Li, G. Wang, X. Wang, Z. Mo, et al., Developing bright afterglow materials via manipulation of higher triplet excited states and relay synthesis in difluoroboron β-diketonate systems, *Adv. Opt. Mater.* (2023) 2302311, <https://doi.org/10.1002/adom.202302311>.
- [57] J. Li, X. Li, G. Wang, X. Wang, M. Wu, J. Liu, et al., A direct observation of up-converted room-temperature phosphorescence in an anti-Kasha dopant-matrix system, *Nat. Commun.* 14 (2023) 1987, <https://doi.org/10.1038/s41467-023-37662-y>.

- [58] H. Yao, Y. Zhang, G. Wang, J. Li, J. Huang, X. Wang, et al., TADF-type organic afterglow nanoparticles with temperature and oxygen dual-responsive property for bimodal sensing, *ACS Appl. Nano Mater.* 6 (2023) 15138–15146, <https://doi.org/10.1021/acsanm.3c02770>.
- [59] D. Li, F. Lu, J. Wang, W. Hu, X.-M. Cao, X. Ma, et al., Amorphous metal-free room-temperature phosphorescent small molecules with multicolor photoluminescence via a host-guest and dual-emission strategy, *J. Am. Chem. Soc.* 140 (2018) 1916–1923, <https://doi.org/10.1021/jacs.7b12800>.
- [60] X. Zhou, X. Zhao, X. Bai, Q. Cheng, Y. Liu, Thermal activated reversible phosphorescence behavior of solid supramolecule mediated by  $\beta$ -cyclodextrin, *Adv. Funct. Mater.* (2024) 2400898, <https://doi.org/10.1002/adfm.202400898>.
- [61] X.-K. Ma, Q. Cheng, X. Zhou, Y. Liu, Macrocycle  $\gamma$ -cyclodextrin confined polymeric chromophore ultralong phosphorescence energy transfer, *JACS Au* 3 (2023) 2036–2043, <https://doi.org/10.1021/jacsau.3c00255>.
- [62] Q. Cheng, X. Ma, X. Zhou, Y. Zhang, Y. Liu, Polymerization based on modified  $\beta$ -cyclodextrin achieves efficient phosphorescence energy transfer for anti-counterfeiting, *Small* (2023) 2309732, <https://doi.org/10.1002/smll.202309732>.
- [63] M. Huo, X. Dai, Y. Liu, Ultrahigh Supramolecular cascaded room-temperature phosphorescence capturing system, *Angew. Chem. Int. Ed.* 60 (2021) 27171–27177, <https://doi.org/10.1002/anie.202113577>.
- [64] W.-L. Zhou, Y. Chen, Q. Yu, H. Zhang, Z.-X. Liu, X.-Y. Dai, et al., Ultralong purely organic aqueous phosphorescence supramolecular polymer for targeted tumor cell imaging, *Nat. Commun.* 11 (2020) 4655, <https://doi.org/10.1038/s41467-020-18520-7>.
- [65] Y.-Y. Liu, X.-Y. Yu, Y.-C. Pan, H. Yin, S. Chao, Y. Li, et al., Supramolecular systems for bioapplications: recent research progress in China, *Sci. China Chem.* 67 (2024) 1397–1441, <https://doi.org/10.1007/s11426-024-1971-4>.
- [66] A. Ryzhakov, T. Do Thi, J. Stappaerts, L. Bertoletti, K. Kimpe, A.R. Sá Couto, et al., Self-assembly of cyclodextrins and their complexes in aqueous solutions, *J. Pharm. Sci.* 105 (2016) 2556–2569, <https://doi.org/10.1016/j.xphs.2016.01.019>.
- [67] F. Nie, K.-Z. Wang, D. Yan, Supramolecular glasses with color-tunable circularly polarized afterglow through evaporation-induced self-assembly of chiral metal-organic complexes, *Nat. Commun.* 14 (2023) 1654, <https://doi.org/10.1038/s41467-023-37331-0>.